Science of the Total Environment 616–617 (2018) 64–72

Contents lists available at ScienceDirect

Science of the Total Environment

journal homepage: www.elsevier.com/locate/scitotenv

Cd isotope fractionation during sulfide mineral weathering in the Fule Zn-Pb-Cd deposit, Yunnan Province, Southwest China

Chuanwei Zhu [a,b], Hanjie Wen [a,*], Yuxu Zhang [a], Runsheng Yin [a], Christophe Cloquet [c]

[a] State Key Laboratory of Ore Deposit Geochemistry, Institute of Geochemistry, Chinese Academy of Sciences, Guiyang 550081, China
[b] Department of Civil and Environmental Engineering, University of Wisconsin–Madison, Madison, WI 53706, USA
[c] Centre de Recherches Petrographiques et Geochimiques, CNRS/UMR 7358, 15, Rue Notre-Dame-Pauvres, B. P. 20, 54501 Vandoeuvre-les-Nancy Cedex, France

HIGHLIGHTS

- Determined Cd isotopic compositions in sulfides and different secondary minerals
- Weathering could result in detectable Cd isotope fractionation ($\Delta^{114/110}Cd \approx 0.33‰$).
- The $\delta^{114/110}Cd$ values and Cd contents decline linearly during weathering.
- Mineral species and grain size control Cd isotope variations in secondary minerals.

GRAPHICAL ABSTRACT

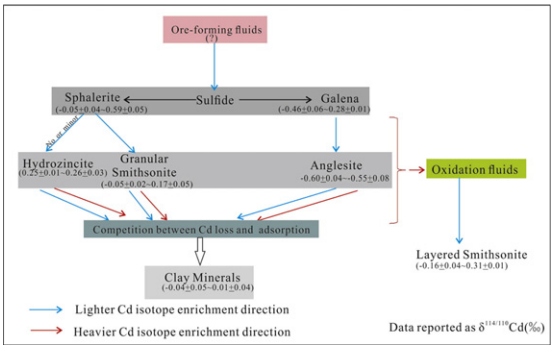

ARTICLE INFO

Article history:
Received 16 July 2017
Received in revised form 26 October 2017
Accepted 28 October 2017
Available online 3 November 2017

Editor: F.M. Tack

Keywords:
Cadmium isotope fractionation
Smithsonite
Anglesite
Hydrozincite
Natural weathering

ABSTRACT

Zinc (Zn)-Lead (Pb) deposits are generally rich in cadmium (Cd), and the weathering of sulfide minerals in such deposits results in large releases of Cd into the environment. From an environmental and public health standpoint, understanding Cd sources and cycling is critical to identifying potential hazards to humans. In this study, the Cd isotope compositions (expressed as $\delta^{114/110}Cd$) of secondary minerals such as anglesite ($-0.57 \pm 0.03‰$; 2 S.D.), granular smithsonite ($0.04 \pm 0.14‰$; 2 S.D.), layered smithsonite ($0.15 \pm 0.40‰$; 2 S.D.), hydrozincite ($0.26 \pm 0.01‰$; 2 S.D.) and clay minerals ($-0.01 \pm 0.06‰$; 2 S.D.) from the Fule Zn-Pb-Cd deposit, Southwest China, are investigated to better understand the Cd sources and cycling in this area.

Combined with our previous study (Zhu et al., 2017), the work herein elucidates the patterns of Cd isotopic fractionation during the formation processes of such secondary minerals and traces the weathering of these minerals into the ecosystem. The $\delta^{114/110}Cd$ values of secondary minerals exhibit the following decreasing trend: hydrozincite > large granular smithsonite > small granular smithsonite > anglesite. Although different amounts of Cd were lost during the formation of equally sized samples, no or minor variations in Cd isotopic composition were observed. However, significant isotopic differences were observed between different size fractions. These results demonstrate that the particle size of secondary minerals and weathering products of sulfide significantly influence Cd isotope composition and fractionation during natural weathering. This systematic fractionation provides an initial foundation for the use of Cd isotopes as environmental tracers in ecosystems and in the global Cd isotope budget.

* Corresponding author.
E-mail address: wenhanjie@vip.gyig.ac.cn (H. Wen).

https://doi.org/10.1016/j.scitotenv.2017.10.293
0048-9697/

1. Introduction

Cadmium (Cd) is a trace heavy metal that is widely distributed in the environment (e.g., Cloquet et al., 2006; Shiel et al., 2012; Lambelet et al., 2013; Wei et al., 2016). This metal is of global concern due to its extreme toxicity to ecosystems and human health (McKenna et al., 1993; Godt et al., 2006; Wiggenhauser et al., 2016). Cadmium acts as a catalyst in the formation of reactive oxygen species (ROS), which in turn increase lipid peroxidation and deplete antioxidants such as glutathione and protein-bound sulfhydryl groups in the human body; ROS also promote the production of inflammatory cytokines (Liu et al., 2009). Exposure to this carcinogenic metal is known to cause health issues ranging from flu-like symptoms to vital liver and kidney damage (Nordberg et al., 1975; Satarug et al., 2003).

Cadmium stable isotope geochemistry is a useful tool for understanding the sources and fates of Cd in the environment. Recent advances in chemical purification techniques and multicollector inductively coupled plasma mass spectrometry (MC-ICP-MS) have enabled the high-precision determination of Cd isotope ratios (Cloquet et al., 2005; Lacan et al., 2006; Ripperger et al., 2007; Schmitt et al., 2009a). To date, large variations in Cd isotopic compositions (~3‰ for $\delta^{114/110}$Cd) have been reported for various geochemical pools, including rocks-minerals, soils-sediments, water and biological samples (Wombacher et al., 2003; Lacan et al., 2006; Ripperger et al., 2007; Schmitt et al., 2009b; Lambelet et al., 2013; Zhu et al., 2015, 2017). Significant mass-dependent fractionation of Cd isotopes can occur during various geochemical processes such as evaporation and condensation (Wombacher et al., 2003, 2004), precipitation (Horner et al., 2011), adsorption (Wasylenki et al., 2014) and biological activity (Lacan et al., 2006; Ripperger et al., 2007; Shiel et al., 2012; Wiggenhauser et al., 2016).

Cadmium has a close relationship with zinc (Zn) due to their similar geochemical properties (McKenna et al., 1993; Schwartz, 2000). Most Zn-Pb deposits contain high levels of Cd (e.g., up to 13.2 wt% in sphalerite, Chmielnicka and Cherian, 1986; Cook et al., 2009; Wen et al., 2015), and the release of Cd from Zn-Pb deposits is a serious environmental issue. The weathering of sulfide minerals releases large amounts of Cd to soils, which further impacts nearby water, plants and animals (Das et al., 1997; Shiel et al., 2012; Wei et al., 2016; Wiggenhauser et al., 2016). Previous studies have reported Cd isotope fractionation during the adsorption of Cd to Mn oxyhydroxide ($\Delta^{114/110}Cd_{fluid\text{-}solid}$: 0.24 to 0.54‰, Wasylenki et al., 2014) and during sulfide ore leaching ($\Delta^{114/110}Cd_{fluid\text{-}solid}$: 0.36 to 0.53‰, Zhang et al., 2016), indicating that Cd isotope fractionation can occur during weathering processes. However, few studies have explored Cd isotope fractionation during natural weathering of Cd-rich sulfide minerals, resulting in a poor understanding of the fates of Cd in Zn-Pb mineralized areas.

In this study, we comprehensively investigated variations in Cd concentrations and isotopic compositions, as well as Zn/Cd ratios, in sulfide minerals (e.g., galena (PbS) and sphalerite (ZnS)) and oxidized secondary minerals (e.g., hydrozincite ($Zn_5(CO_3)_2(OH)_6$), smithsonite ($ZnCO_3$) and anglesite ($PbSO_4$)) from the Fule Zn-Pb-Cd deposit in Southwest China to better understand the fate of Cd during weathering processes.

2. Methods

2.1. Site description

The Fule deposit is a representative Mississippi Valley-Type (MVT) Zn-Pb-Cd ore deposit in the south-eastern region of the Sichuan-Yunnan-Guizhou (SYG) triangle area in Southwest China. This deposit is primary located in the Lower Permian Maokou Formation (P_1m), which predominantly comprises grey (dark to light grey) dolomitic limestone (Fig. 1). Details of the geological setting were previously reported (Zhu et al., 2017). The Fule Zn-Pb deposit consists primarily of sulfide minerals such as galena and sphalerite that have been shown to contain extremely high Cd concentrations (5238 to 34,981 μg/g); the stock of Cd in the deposit is about 4500 tons (Zhu et al., 2017), posing a health risk to local populations and living organisms. In the Fule deposit, oxidized layers contain hydrozincite, smithsonite, anglesite and clay minerals (Fig. 2), which are commonly believed to have formed during the weathering of sulfide deposits located near or directly above these layers (Takahashi, 1960). The smithsonite formed as a result of sphalerite oxidation, and both granular and layered smithsonite were found in the weathered layer.

Sulfides including galena (n = 7) and sphalerite (n = 14) were collected from the Fule deposit (for detailed information, please see Zhu et al., 2017). During our sampling campaign, hydrozincite (n = 2), granular smithsonite (n = 7), layered smithsonite (n = 1), anglesite (n = 3) and clay minerals (n = 2) were also collected from the closest oxidized layer, which has a depth of about 1 m and an area of about 100 m^2 (Fig. 2). Detailed information about the samples is summarized in supplementary figures (Appendix A.1).

In the laboratory, each sample was dried (40 °C). Sample FL-16 was divided using various mesh sieves into four groups: mass (particle size > 10 mm; FL-16-3), 10-mesh (sieve size: 2.00 mm; FL-16-4), 20-mesh (sieve size: 0.85 mm; FL-16-5) and 40-mesh (sieve size: 0.43 mm; FL-16-6). Because the particles in FL-15 were relatively small, this sample was divided into two groups: 10-mesh (FL-15-1) and 20-mesh (FL-15-2). Two unoxidized sphalerite samples (FL-16-1 and FL-16-2) were separated from the mass oxidized ores in FL-16, which are used as proxies for the initial Cd isotope composition in these oxides (Appendix A.1). Meanwhile, two samples (FL-15-2 and FL-5) were selected as duplicates to monitor the chemical separation and isotope analyses.

2.2. Cadmium adsorption and mineralogy measurements

The heavy metal desorption method recommended by Chen et al. (2008) was adopted for analysis of the total Cd adsorption in oxides. After crushing to <74 μm (200 mesh), triplicates of the FL-16-3 (mass oxide) sample were weighed (n = 3, 1 g each) into 50 mL polypropylene centrifuge tubes. The three samples were then reacted with either 25 mL ultra-pure water, 25 mL 500 mmol/L NaCl or 25 mL 1000 mmol/L NaCl. After shaking for 2 h, the tubes were placed in a oven and heated at 25 °C for another 24 h. The tubes were then centrifuged (at 4000 rpm) for 20 min, and 2 mL of the supernatant were used for the total Cd adsorption measurement. In addition, all samples were analysed by XRD (X-ray diffraction) and/or EPM (Electron Probe Microanalysis) to investigate the mineralogy of the oxides.

2.3. Concentration and isotopic composition analyses

All samples were crushed to <74 μm prior to chemical analysis. The Cd and Zn concentrations in a ~0.1 g portion of each sample were measured using a Varian Vista MPX inductively coupled plasma optical emission spectrometer (ICP-OES) at the State Key Laboratory of Ore Deposit Geochemistry at the Institute of Geochemistry of the Chinese Academy of Sciences. Cadmium isotope ratios were measured using a Thermo-Finnigan Neptune Plus MC-ICP-MS. Detailed methodological information (e.g., sample preparation, Cd separation and purification, and isotopic determination) were reported previously (Zhu et al., 2017). Isotopic data are reported as δ values in units of per mille (‰) and referenced to the Nancy Spex Cd reference standard (which was analysed before and after each sample):

$$\delta^{114/110}\mathrm{Cd}(‰) = \left[\left(\left({}^{114}\mathrm{Cd}/{}^{110}\mathrm{Cd}\right)_{\mathrm{sample}}/\left({}^{114}\mathrm{Cd}/{}^{110}\mathrm{Cd}\right)_{\mathrm{std}} - 1\right] \times 1000 \quad (1)$$

Münster Cd solution and NIST SRM 3108 Cd solution were used as secondary reference standards; these solutions were previously reported to have $\delta^{114/110}$Cd values of 4.50 ± 0.08 (2 S.D., N = 31) and 0.11 ±

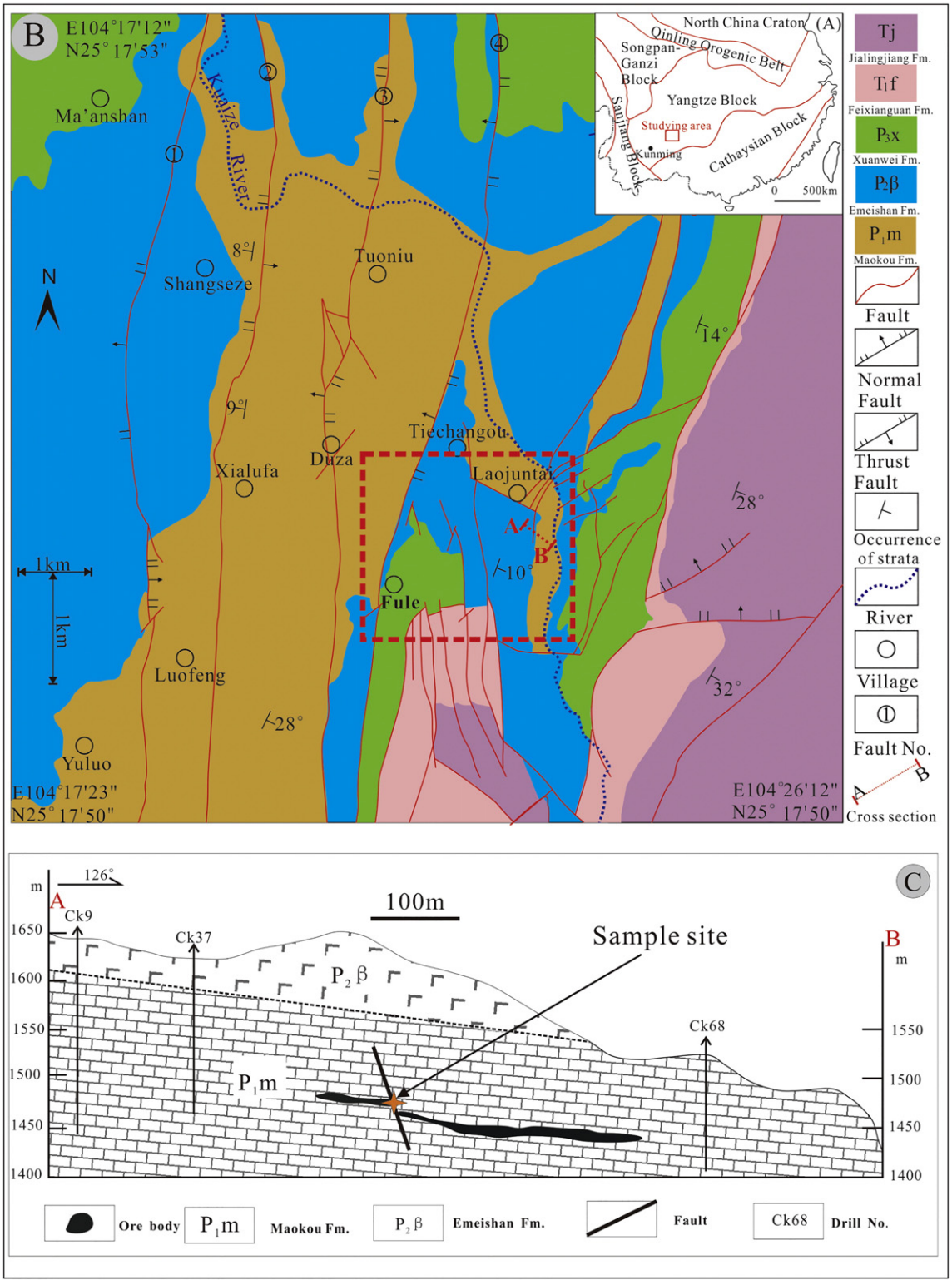

Fig. 1. (A) Diagram of the tectonic framework of South China. Plan views of the (B) orebodies and (C) cross-section of the Fule deposit (modified after data up to 1994 from the Fule Mine). Tj: the Jialingjiang Formation; T_1f: the Feixianguan Formation; P_{3x}: the Xuanwei Formation; $P_2\beta$: the Emeishan Formation and P_{1m}: the Maokou Formation.

0.03 (2 S.D., N = 30) respectively (Zhang et al., 2016), which agree well with other previous reference standard results. The long-term instrumental reproducibility of our method is <0.05‰ (2 S.D.) for $\delta^{114/110}Cd$.

In this study, Cd isotopic data are also reported and discussed relative to the NIST SRM 3108 Cd isotope standard using the equation: $\delta^{114/110}Cd_{NIST\text{-}SRM\text{-}3108} = \delta^{114/110}Cd_{Nancy\text{-}Spex} - 0.11$ (Table 2).

3. Results and discussion

3.1. Mineralogy in the Fule sulfide deposit and weathered layer

Major minerals were identified using XRD and EPM in both the sulfide and oxidized samples. Sphalerite (ZnS), galena (PbS) and calcite ($CaCO_3$) have been previously identified as the major minerals in the

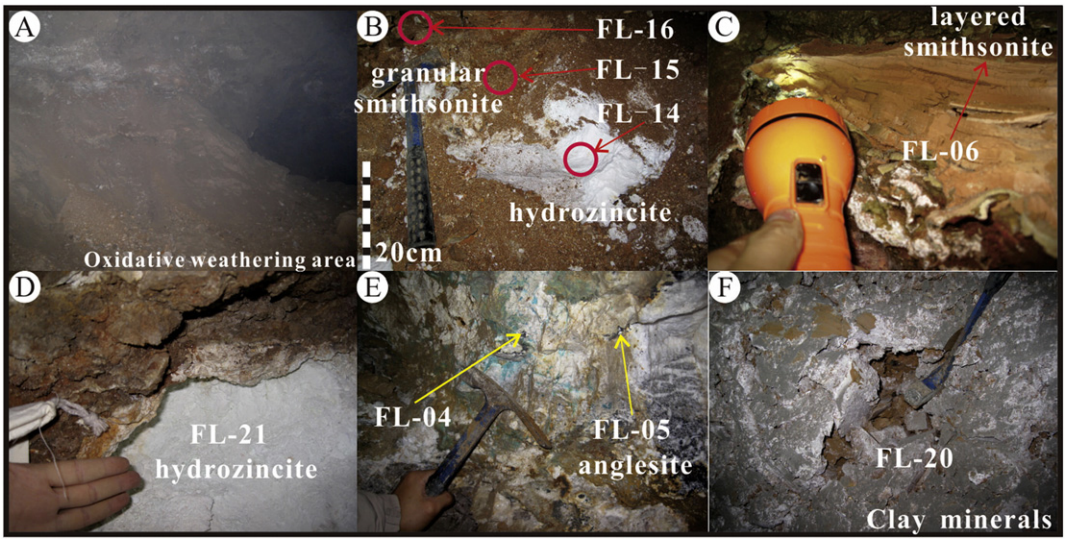

Fig. 2. Photographs of the sections at the oxides sample locations: (A) Overall view of the oxidative weathering area; (B–F) close-up images of the different sampling sites.

Fule deposit (Zhu et al., 2017). However, the weathered layer contains primarily hydrozincite ($Zn_5(CO_3)_2(OH)_6$ or $Zn_5(OH)_6(CO_3)_2$), smithsonite ($ZnCO_3$), anglesite ($PbSO_4$) and clay minerals, which are secondary minerals formed during sulfide mineral weathering. Massive and granular smithsonites commonly have sphalerite residuals, while layered smithsonites are relatively pure, having been formed by the precipitation of dissolved smithsonites (Zhu et al., 2017). From a geochemical perspective, hydrozincite ($Zn_5(CO_3)_2(OH)_6$) and smithsonite ($ZnCO_3$) result from sphalerite (ZnS) weathering, while anglesite ($PbSO_4$) is formed from the weathering of galena (PbS). The oxidation of sulfide minerals (galena and sphalerite) can be described by the following simplified reaction equations (e.g., Podda et al., 2000; Urbano et al., 2007; Heidel et al., 2011, 2013):

$$ZnS + 2O_2 \rightarrow Zn^{2+} + {SO_4}^{2-} \quad (2)$$

$$PbS + 2O_2 \rightarrow Pb^{2+} + {SO_4}^{2-} \rightarrow PbSO_{4(s)} \quad (3)$$

$$Zn^{2+} + {CO_3}^{2-} \rightarrow ZnCO_{3(s)} \quad (4)$$

$$Zn^{2+} + {CO_3}^{2-} + 6H_2O \rightarrow Zn_5(CO_3)_2(OH)_{6(s)} + 6H^+ \quad (5)$$

Limestone dissolution ($CaCO_3 \rightarrow Ca^{2+} + CO_3^{2-}$) and water-rock reactions during weathering can release CO_3^{2-} in O_2-rich waters, which facilitates the oxidation of sphalerite and galena (Appendix A.2). Under natural conditions, clay minerals have been observed in secondary precipitates and in the secondary phase on the slag surface (Ettler et al., 2001). Simulation experiments also show the formation of silicate minerals on sphalerite surfaces during sphalerite oxidation (Heidel et al., 2011). In this study, we find that clay minerals replace secondary minerals (e.g., anglesite and smithsonite; Appendix A.2, Figs. E and F); it is therefore reasonable to conclude that clay minerals are the final products of the weathering sequence.

Based on previous studies (Heidel et al., 2011, 2013), secondary minerals can be organized by their different formation sequences during weathering processes. Sulfide oxidation experiments show that galena is more reactive and easily oxidized than sphalerite (Silva et al., 2003; Heidel et al., 2011, 2013), indicating that anglesite was formed before other secondary minerals. Back-scattered electron (BSE) images show that sphalerite is replaced by smithsonite to form smithsonite aggregates, suggesting that sphalerite can be directly oxidized into smithsonite (Appendix A.2, Fig. A). No sphalerite particles or residuals were observed in hydrozincite, which also featured banded texture (Appendix A.2, Fig. B), suggesting that hydrozincite was precipitated from Zn oxidized leachates and that granular smithsonite was formed before hydrozincite. This conclusion is supported by the presence of hydrozincite at the bottom of the oxidation profile (Fig. 2B). Both hydrozincite and layered smithsonite were precipitated from Zn oxidized leachates in the Fule deposit (Zhu et al., 2017), but the formation sequence of hydrozincite and layered smithsonite remains unclear. Overall, the minerals in the Fule deposit were formed in the following sequence: sulfides (sphalerite and galena) > anglesite > granular smithsonite > hydrozincite and/or layered smithsonite > clay minerals.

3.2. Cd and Zn concentrations in secondary minerals

The transformation of sulfides to secondary minerals during weathering processes results in Cd mobilization and redistribution. This is evidenced by the lower Cd concentrations in secondary minerals as compared to sphalerites which have Cd concentrations of 5238 to 34,981 μg/g (with an average of 18,081 μg/g). However, the sphalerites have significantly higher Cd concentrations than the galenas (48 to 1163 μg/g; mean = 367 μg/g), suggesting that sphalerite is the main Cd host in the Fule deposit (Zhu et al., 2017; Wen et al., 2016). In the weathered layer, Cd concentrations vary greatly in layered smithsonite (6216 to 13,308 μg/g; mean = 8865 μg/g), granular smithsonite (1318 to 19,963 μg/g; mean = 7199 μg/g) and hydrozincite (1888 to 4888 μg/g; mean = 3388 μg/g). In general, Cd concentrations in secondary minerals are lower than those in sphalerites but higher than those in galenas. The high Cd concentrations in sulfide and secondary minerals suggest high environmental risk for Cd pollution (Table 2, Fig. 3).

Cadmium in geological samples occurs mainly as (1) independent minerals such as greenockite (CdS) and otavite ($CdCO_3$, Urbano et al., 2007; Lattanzi et al., 2010; Chrastný et al., 2015), (2) isomorphic forms (Schwartz, 2000; Tu et al., 2004; Frost et al., 2008; Ye et al., 2011) and (3) that adsorbed onto the mineral surfaces (Tu et al., 2004; Wasylenki et al., 2014). XRD analysis shows that granular smithsonite samples consist primarily of smithsonite associated with minor anglesite (Appendix A.2). Detailed field and BSE analyses also indicate a lack of independent Cd minerals. Our desorption experiments show that, with increased solution NaCl concentration, the desorbed Cd increased from 156 to 439 μg (Table 1), which accounts for <0.02% of the total Cd in the sample (19,963 μg/g). Taken together, this suggests that the Cd in the Fule samples exists mainly in isomorphic forms rather than in independent or adsorbed mineral forms. The geochemical properties of Cd are similar to those of Zn due to similarities in their electron structures and ionization potentials; Cd occurs in Zn ores largely

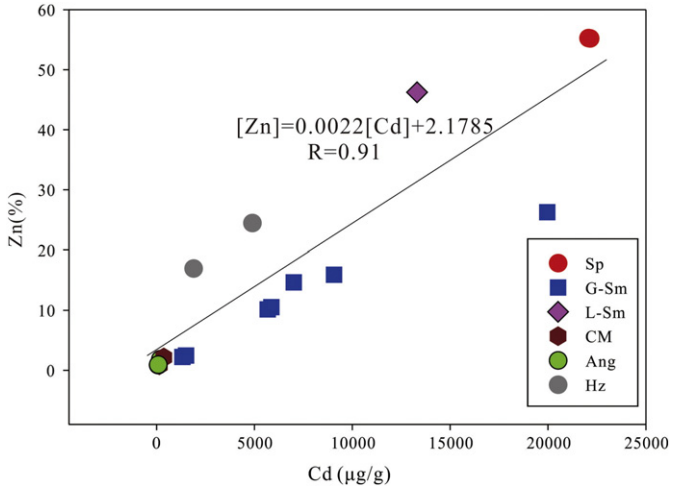

Fig. 3. Relationship between Zn (%) and Cd (μg/g) concentrations in studied samples from the Fule deposit. Sph = sphalerite; G-Sm = granular smithsonite; L-Sm = layered smithsonite; CM = clay minerals; Ang = anglesite; Hz = hydrozincite.

through $Cd^{2+} \rightarrow Zn^{2+}$ substitution (Cook et al., 2009; Ye et al., 2011). A positive linear correlation ($R^2 = 0.91$) between Cd and Zn concentrations was observed in all of the samples presented herein (Fig. 3), supporting our hypothesis that Cd is present predominantly in isomorphic forms, as this positive correlation would likely not occur if Cd were primarily adsorbed or present in the independent Cd mineral form.

3.3. Zn/Cd ratios in secondary minerals

Although the geochemical similarities of Zn and Cd caused a general positive correlation between Zn and Cd in samples, slight differences in Zn/Cd ratios can exist among samples due to differences in Zn and Cd mobility (Tu et al., 2004; Udovic and Lestan, 2009; Souissi et al., 2013). There is overlap between the Zn/Cd ratios of sphalerites (17 to 120) and galenas (11 to 63); however, sphalerites and galenas show distinct mean Zn/Cd ratios (of 43 and 31, respectively), suggesting different partitioning of Zn and Cd in various sulfides. Compared to sphalerites (the proposed leading source of Cd in the weathered layer; mean = 25 ± 0), secondary minerals have more variable Zn/Cd ratios (Fig. 4). Except for granular smithsonites (mean = 17 ± 5, 2 S.D., n = 7), most of the secondary minerals, including hydrozincite (70 ± 56, 2 S.D.; n = 2); layered smithsonite (mean = 58 ± 38, 2 S.D., n = 5), anglesite (mean = 110 ± 21; n = 3) and clay minerals (mean = 60 ± 1, 2 S.D., n = 2), have higher Zn/Cd ratios than mean Zn/Cd ratios of the sphalerite. Differences in Zn/Cd ratios between sphalerites and secondary minerals indicate variable Zn and Cd partitioning during weathering. It has been proposed that Cd and Zn possess different mobilities during the formation of such secondary minerals (Fuge et al., 1993; Gerringa et al., 2001; Udovic and Lestan, 2009; Souissi et al., 2013).

3.4. Cd isotope fractionation in hydrozincite and anglesite

In the Fule deposit, the Cd isotopic composition variations in sphalerites ($\delta^{114/110}$Cd: −0.05 to 0.59‰) and galenas ($\delta^{114/110}$Cd: −0.46 to 0.28‰, Table 2 and Fig. 4) have been explained by Rayleigh-type isotopic fractionation in the hydrothermal system, which results in lower $\delta^{114/110}$Cd values in minerals with earlier formation dates (Wen et al., 2016; Zhu et al., 2017).

The $\delta^{114/110}$Cd values are variable among secondary minerals (Fig. 4). The $\delta^{114/110}$Cd value ranges for granular smithsonite (−0.05 to 0.17‰) and hydrozincites (0.25 to 0.26‰) are within that for sphalerites (−0.05 to 0.59‰, Zhu et al., 2017). Hydrozincites have quite consistent $\delta^{114/110}$Cd values (0.26 ± 0.01‰, 2 S.D.; n = 2), which are similar to sphalerite $\delta^{114/110}$Cd values in both the oxidation profile (0.28 ± 0.03‰, 2 S.D.; n = 2) and the Fule sulfide deposit (in which the mean value is 0.29‰, n = 14, Fig. 4B). Therefore, we hypothesize that limited Cd isotope fractionation occurred during the weathering of sphalerite to hydrozincite. Although previous studies have shown Cd isotope fractionation during Cd adsorption ($\Delta^{114/110}Cd_{fluid\text{-}solid}$: 0.24 to 0.54‰, Wasylenki et al., 2014) and during sulfide ore leaching ($\Delta^{114/110}Cd_{fluid\text{-}solid}$: 0.36–0.53‰, Zhang et al., 2016), isotope fractionation is unlikely to be observed if the process has been completed. Zinc and Cd are thought to be released completely from weathered sphalerite; the released Zn later forms hydrozincites, with Cd^{2+} present as an isomorphism of Zn^{2+}. It is likely that little Zn or Cd was lost during weathering processes, as 1) the host limestone should provide enough CO_3^{2-} for the formation of carbonate minerals such as hydrozincite and 2) the Cd^{2+} activity decreased approximately 100-fold under alkaline conditions (Street et al., 1977). We propose that most of the Cd was incorporated into hydrozincite during the weathering of sphalerite, resulting in limited Cd isotope fractionation between sphalerite and hydrozincite.

Anglesites have $\delta^{114/110}$Cd values (−0.57 ± 0.04‰, 2 S.D.; n = 3) significantly lower than those of the parent galenas in the sulfide deposit (Fig. 4). The mean $\delta^{114/110}$Cd values of anglesites and galenas differ by 0.5‰ (Fig. 4), which is similar to the reported fractionation of Cd isotopes during sulfide ore leaching ($\Delta^{114/110}Cd_{fluid\text{-}solid}$: 0.36–0.53‰, Zhang et al., 2016). This suggests that heavier Cd isotopes were preferentially lost during the weathering of galena to anglesite. Generally, $CdSO_4$ is more soluble than $CdCO_3$; therefore, heavy Cd isotopes are more easily lost during the weathering of galena (as compared to sphalerite weathering), resulting in relative enrichment of light Cd isotopes in anglesite ($\delta^{114/110}$Cd = −0.57 ± 0.04‰, 2 S.D.; n = 3). Meanwhile, geochemical and isotopic data suggest that the large galena-mass-to-water volume ratio caused a rapid saturation of the solution with anglesite (Heidel et al., 2013); thus, this process could result in large Cd isotope fractionation due to the kinetic fractionation effect. Taken together, we presume that high $CdSO_4$ solubility and rapid precipitation of anglesite are the two primary factors driving Cd isotopic signatures in anglesite.

3.5. Cd isotope fractionation in smithsonite and clay

Data from this study and Zhu et al. (2017) indicate that layered smithsonites from the Fule deposit have large Cd isotope fractionations ($\Delta^{114/110}$Cd = 0.47‰) with $\delta^{114/110}$Cd values ranging from −0.16 to 0.31‰. These data are negatively correlated to Cd concentrations ($R^2 = 0.86$, n = 5), while Zn/Cd ratios and $\delta^{114/110}$Cd values are positively correlated ($R^2 = 0.85$, n = 5, Fig. 5). Using the sampling sites and ore textures, Zhu et al. (2017) established the precipitation sequence of layered smithsonite, finding that light Cd isotopes are enriched in precipitated smithsonites with earlier formation dates

Table 1
Oxide desorption experiments.

	Sample weight	Cd concentration	Desorption matrix	Solution volume	Desorbed quantity of Cd	Desorption rate
	g	μg/g		mL	μg	%
Experiment 1	0.9998	19,963	Ultra-pure water	25	156	0.008
Experiment 2	0.9969	19,963	500 mmol/L NaCl	25	286	0.014
Experiment 3	0.9929	19,963	1000 mmol/L NaCl	25	439	0.022

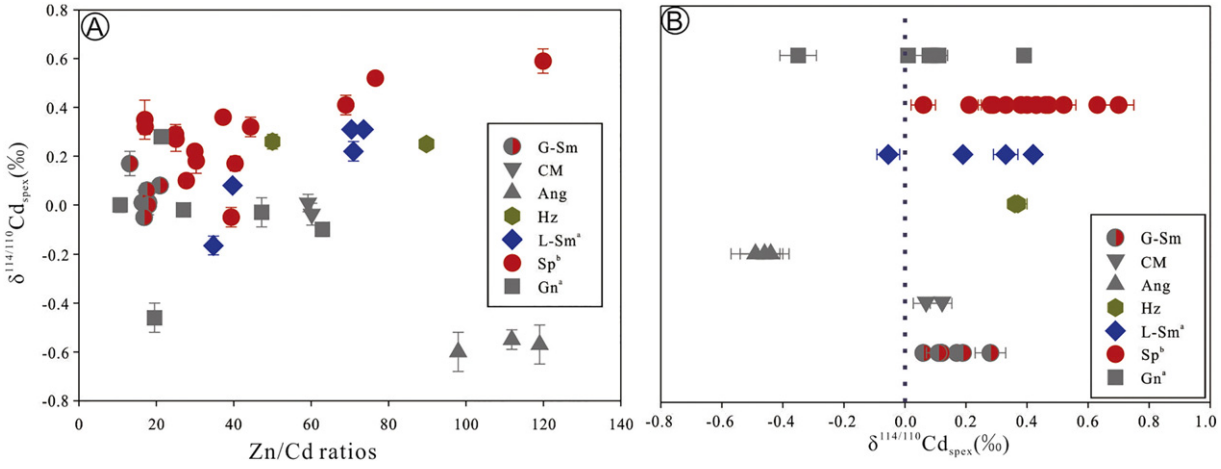

Fig. 4. Plots of (A) $\delta^{114/110}Cd_{spex}$ vs. Cd/Zn ratio and (B) Cd isotope distributions in samples from the Fule deposit. Data for sphalerite and galena are from Wen et al. (2016) and Zhu et al. (2017), respectively. Sph = sphalerite; G-Sm = granular smithsonite; L-Sm = layered smithsonite; CM = clay minerals; Ang = anglesite; Hz = hydrozincite.

(Fig. 5). This is consistent with previous studies showing that light Cd preferentially partitions into the solid phase rather than the solution (Horner et al., 2011; Yang et al., 2014).

BSE images show that anglesite is surrounded by smithsonite in granular smithsonite samples (Appendix A.2). Thus, it is important to elucidate the origins of Cd in granular smithsonite samples. As mentioned previously, Cd occurs chiefly in Zn minerals, with high Cd concentrations in granular smithsonite and layered smithsonite. Cadmium concentrations in anglesite (<100 μg/g) are much lower than those in granular smithsonite (>1000 μg/g) and layered smithsonite (>5000 μg/g, Table 2). Thus, Cd in anglesite is negligible compared to that in smithsonite, which is the major Cd source in granular smithsonite samples. Interestingly, Cd and Zn concentrations decrease with decreasing particle size (Table 2), and, in granular smithsonite, $\delta^{114/110}$Cd values are closely related to grain particle size. It is proposed that the lighter Cd isotopes were concentrated in the smaller particles.

In the oxidation profiles, the FL-16 samples are close to the FL-15 and FL-14 samples. Primary sphalerite (FL-16-1 and FL-16-2) can be assumed to represent the primary Cd isotopic composition of the oxidation system. This assumption is explained as follows: (1) although sphalerite samples from the Fule deposit have large Cd isotope fractionation ($\Delta^{114/110}$Cd = 0.64‰) and large Cd concentration variations (5238 to 34,757 μg/g), the average $\delta^{114/110}$Cd value (mean = 0.29 ± 0.36‰; 2 S.D., n = 12) and Cd concentration (mean = 17,410 ± 18,596 μg/g; 2 S.D., n = 12) from published sphalerite data (Zhu et al., 2017) are similar to those of samples FL-16-1 and FL-16-2 (Table 2); (2) Samples FL-16-1 and FL-16-2, which were separated from the same hand specimen, displayed no differences in Cd isotope fractionation, indicating that the Cd isotope distribution is homogeneous at a small scale, which is consistent with previous studies (Zhu et al., 2017). As mentioned above, the supergene mineral parent sphalerites from the oxidation profile are geochemically similar to the unoxidized sphalerites (FL-16-1 and FL-16-2). Thus, we propose that the oxidative weathering of sphalerite could result in significant Cd isotope fractionation, with $\Delta^{114/110}Cd_{sphalerite\text{-}smithsonite}$ values up to 0.33‰. The data also show that $\delta^{114/110}$Cd is positively correlated with Cd concentration (R^2 = 0.92, Fig. 6), which could be explained by either equilibrium or kinetic fractionation; these two mechanisms have different implications, but unfortunately cannot be distinguished using currently available means. However, regardless of whether the observations result from equilibrium or Rayleigh fractionation, another important observation must be discussed. The magnitude of fractionation in the

Table 2
Cadmium isotopic compositions of various samples from the Fule deposit.

Sample no	Sample type	Cd(μg/g)	Zn(%)	Zn/Cd	$\delta^{114/110}$Cd	2σ	$\delta^{112/110}$Cd	2σ	$\delta^{114/110}$Cd[b]
FL-16-1	Sp	22,151	55.21	25	0.40	0.04	0.21	0.01	0.29
FL-16-2	Sp	22,064	55.26	25	0.38	0.05	0.19	0.01	0.27
FL-16-3	G-Sm (mass)	19,963	26.26	13	0.28	0.05	0.14	0.03	0.17
FL-16-4	G-Sm(10 mesh)	9066	15.91	18	0.17	0.03	0.08	0.01	0.06
FL-16-5	G-Sm (20 mesh)	1504	2.47	16	0.12	0.05	0.06	0.03	0.01
FL-16-6	G-Sm(40 mesh)	1318	2.22	17	0.06	0.02	0.03	0.01	−0.05
FL-15-1	G-Sm (10 mesh)	7004	14.65	21	0.19	0.02	0.10	0.01	0.08
FL-15-2	G-Sm(20 mesh)	5863	10.53	18	0.12	0.05	0.06	0.03	0.01
	Duplicate	5677	10.15	18	0.11	0.01	0.05	0.00	0.00
FL-7	Clay (200 mesh)	140	0.84	60	0.07	0.05	0.04	0.02	−0.04
FL-20	Clay (201 mesh)	363	2.15	59	0.12	0.04	0.07	0.02	0.01
FL-4	Anglesite	189	1.85	98	−0.49	0.08	−0.25	0.04	−0.60
FL-5	Anglesite	78	0.87	112	−0.44	0.04	−0.23	0.01	−0.55
	Duplicate	80	0.95	119	−0.46	0.08	−0.24	0.02	−0.57
FL-21	Hydrozincite	1888	16.95	90	0.36	0.01	0.18	0.00	0.25
FL-14	Hydrozincite	4888	24.44	50	0.37	0.03	0.19	0.03	0.26
FL-6	L-Sm	13,308	46.24	35	−0.05	0.04	−0.02	0.01	−0.16
SBFL-05[a]	L-Sm(early)	12,128	48.14	39.69	0.19	0.01	0.06	0.01	0.08
SBFL-05[a]	L-Sm(middle)	6283	44.57	70.94	0.33	0.04	0.15	0.01	0.22
SBFL-05[a]	L-Sm(late)	6216	45.72	73.55	0.42	0.01	0.20	0.01	0.31
SBFL-05[a]	L-Sm(late)	6389	45.00	70.43	0.42	0.01	0.20	0.01	0.31

Note: Sp, sphalerite; G-Sm, granular smithsonite; Ang, anglesite; Hz, hydrozincite; L-Sm, layered smithsonite; the particle size of mass granular smithsonite (FL-16-3) is over 10 mm.
[a] Reported by Zhu et al. (2017).
[b] Reported relative to NIST-SRM-3108.

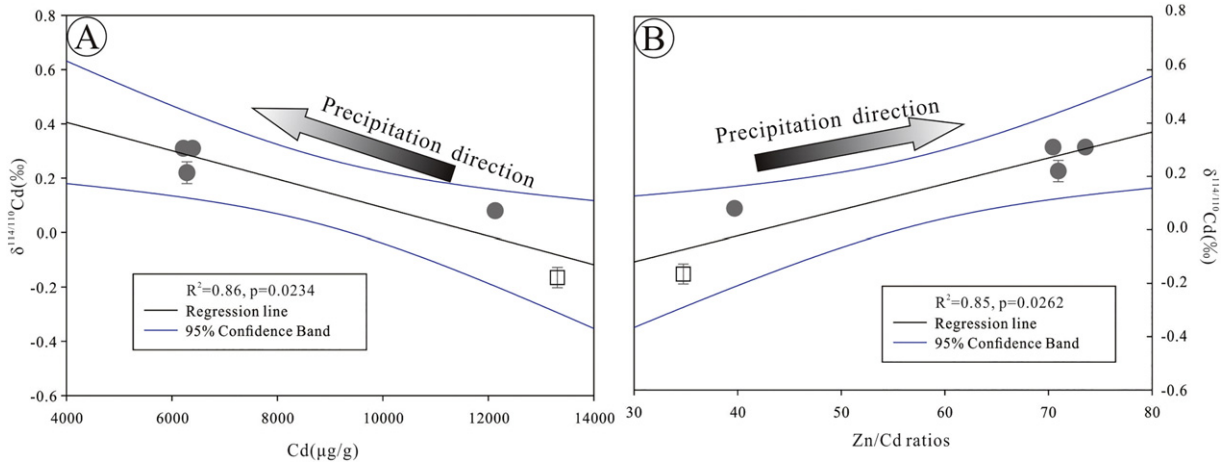

Fig. 5. Correlations between $\delta^{114/110}$Cd and (A) Cd concentration and (B) Cd/Zn ratio in early- to late-stage smithsonite. Data for layered smithsonite (black filled circles) are from Zhu et al. (2017).

particle series shows an unequivocal increase with specific surface area from mass to clay samples, with $\delta^{114/110}$Cd values varying from +0.17 to −0.05‰. One explanation for this observation is that the Cd isotopes in the small particle samples were influenced by the Cd isotopes in the oxidative fluids; thus, the small particle samples were dominated by the Cd isotope composition of the oxidative fluids. However, with decrease of specific surface area, it is harder for the Cd isotopes in larger particle samples (e.g., mass samples) to equalize with those in oxidative fluids; thus, the Cd isotope signature in large particle samples is inherited primarily from that of the parent sphalerite. Notably, in a comparison of Cd concentrations between clay samples, 10- and 20-mesh samples (Table 2) show Cd concentration variations in samples with the same particle size, suggesting different amounts of Cd loss during weathering processes. Generally, samples with lower Cd concentrations have lower $\delta^{114/110}$Cd values (Fig. 6A). However, no significant variations in Cd isotopic composition were observed between particle samples of equal size (e.g., FL-16-4 and Fl-15-1). These results demonstrate that although oxidative weathering results in different amounts of Cd loss, Cd isotopes are homogeneously distributed in samples of consistent particle size. This conclusion supports the hypotheses that Cd isotopes in samples with small particle size were equalized with those in oxidative fluids, and that fractionation in secondary minerals may be an equilibrium effect.

Electron probe analysis (Appendix A.2) shows smithsonite and anglesite particles (~1 μm) surrounded by clay minerals, indicating that clays may be considered the final product of sulfide oxidation. According to the relationships between Cd and its isotope compositions during weathering (Fig. 6), the calculated $\delta^{114/110}$Cd value of clay is −0.07‰, which lower is than those in all granular smithsonites. However, the measured $\delta^{114/110}$Cd values of clay (−0.04 to +0.01‰) are slightly higher than those in 40-mesh granular smithsonite (−0.05‰, Table 2) and the calculated value (−0.07‰); thus, a different mechanism must be responsible. Although Cd in clay samples occurs mainly in Zn minerals, Cd sorption in clay minerals must also be considered (Bittell and Miller, 1974). Wasylenki et al. (2014) suggested that heavier Cd isotopes are adsorbed more readily during Cd sorption to synthetic birnessite. Thus, Cd sorption can potentially yield somewhat higher $\delta^{114/110}$Cd values, as observed in the clay samples in this study.

3.6. Implications for the application of Cd isotopes in the environment

Sulfides, and especially sphalerite, are the most common Cd-bearing minerals on Earth. Our assessment of the Cd isotope fractionation from sulfides into different secondary minerals provides an additional constraint and environmental tracer for the global Cd isotope budget.

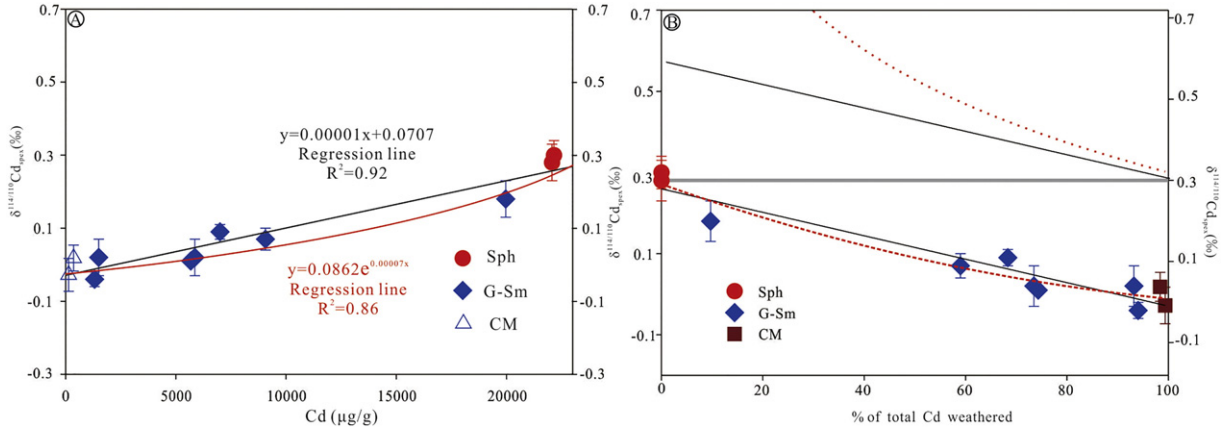

Fig. 6. (A) Relationship between $\delta^{114/110}Cd_{spex}$ and Cd abundance for granular smithsonite (G-Sm), clay minerals (CM), and sphalerite (Sph). (B) Isotopic compositions of Cd in fluids and solids versus the loss of Cd in the sample with respect to the original Cd concentration for sphalerites (FL-16-1 and FL-16-2). We assume that $f = (Cd_{sphalerite} - Cd_{residual}) / Cd_{sphalerite}$ and that the isotopic fractionation factor (α) for Cd lost during weathering is $\alpha_{sulfide\text{-}solution} = 0.99967$, which is similar to that for Cd precipitated into calcite ($\alpha = 0.99955 \pm 0.00012$, Horner et al., 2011). The solid lines are linear best fits (implying closed-system equilibrium fractionation), and the dashed lines are Rayleigh fractionation curves with a fractionation of $\Delta^{114/110}$Cd = 0.33‰.

Numerous studies have focused on Cd isotope fractionation during Zn and Pb mining, smelting and refining and in the environment surrounding these facilities (Cloquet et al., 2006; Shiel et al., 2010, 2012; Chrastný et al., 2015; Wen et al., 2015; Zhang et al., 2016; Martinková et al., 2016), but fewer have used Cd isotopes to track Cd sources in Cd-polluted soils in different Zn-Pb mining areas (Cloquet et al., 2006; Wen et al., 2015; Zhang et al., 2016). This work presents further study of oxidative weathering processes that result in significant Cd isotope fractionation and that have not been examined in the literature to date. Additionally, our results are among the first to describe relationships between particle size and $\delta^{114/110}$Cd values and between different secondary minerals, which may significantly influence Cd isotope fractionation. Future studies should incorporate the relationships between sample size and Cd isotope composition found herein when using Cd isotopes to trace Cd pollution sources in mining areas.

The main Cd input and removal fluxes to and from the ocean have been estimated, and rivers are thought to be the most important source of marine Cd (Duce et al., 1991; Horner et al., 2011). Meanwhile, rivers and seawater are reported to be enriched in heavy Cd isotopes in comparison to bulk silicate earth (Zhu et al., 2015, and reference therein), suggesting that seawater and river water are reservoirs of heavy Cd isotopes. Zn-Pb deposits are considered to be one of the most important Cd reservoirs on Earth, and sulfide weathering results in large amounts of Cd release (enriched in heavy isotopes) into environments and ecosystems. Although biological activity was thought to be the primary factor resulting in modern ocean heavy isotope enrichment, our study suggests that weathering could also contribute appreciably to heavy Cd isotope enrichment in riverine and marine environments.

4. Conclusions

In summary, our investigation of Cd concentrations and isotopic compositions in different secondary minerals from the Fule deposit resulted in the following conclusions:

(1) Cd has a positive correlation with Zn in the studied samples. Based on electron microprobe and XRD analysis and desorption experiments, we suggest that Cd was incorporated into the studied samples predominantly by direct substitution of Zn^{2+} by Cd^{2+}.
(2) For layered smithsonite, Cd concentrations decreased from early to late stages, while $\delta^{114/110}$Cd values increased; this indicates that Cd and its light isotopes are preferentially enriched in early precipitation.
(3) For granular smithsonite, Cd concentration is positively correlated with $\delta^{114/110}$Cd value. Light Cd isotopes are preferentially enriched during weathering in samples with small particle sizes. Although oxidative weathering results in varying amounts of Cd loss in samples with similar particle sizes, the Cd isotope ratios in those samples are homogenous. These results indicate that particle size may significantly influence Cd isotope fractionation. We also propose that adsorbed Cd in clay samples may result in $\delta^{114/110}$Cd values in clay samples higher than those in 40-mesh granular smithsonite.
(4) We investigated the Cd isotope compositions in different secondary minerals and found the following trend in light Cd isotope enrichment: anglesite > small particle granular smithsonite > large particle granular smithsonite > hydrozincite, which indicates that different weathering processes may significantly influence Cd isotope fractionation.

Acknowledgments

This work was financially supported by the National Natural Science Foundation of China (Nos. 41503011, 41573007), Science and Technology Foundation of Guizhou Province ([2016]1159). Four anonymous reviewers and editor Filip M.G. Tack are hereby acknowledged for their thoughtful comments, which have significantly improved this manuscript.

Appendix A. Supplementary data

Supplementary data to this article can be found online at https://doi.org/10.1016/j.scitotenv.2017.10.293.

References

Bittell, J.E., Miller, R.J., 1974. Lead, cadmium, and calcium selectivity coefficients on a montmorillonite, illite, and kaolinite. J. Environ. Qual. 3 (3), 250–253.
Chen, S., Sun, L.N., Chao, L., Sun, T.H., 2008. Effects of inorganic anions on the desorption character of cadmium, lead. Ecol. Environ. 17, 105–108 (in Chinese with English abstract).
Chmielnicka, J., Cherian, M.G., 1986. Environmental exposure to cadmium and factors affecting trace-element metabolism and metal toxicity. Biol. Trace Elem. Res. 10 (3), 243–262.
Chrastný, V., Čadková, E., Vaněk, A., Teper, L., Cabala, J., Komárek, M., 2015. Cadmium isotope fractionation within the soil profile complicates source identification in relation to Pb–Zn mining and smelting processes. Chem. Geol. 405, 1–9.
Cloquet, C., Rouxel, O., Carignan, J., Libourel, G., 2005. Natural cadmium isotopic variations in eight geological reference materials (NIST SRM 2711, BCR 176, GSS-1, GXR-1, GXR-2, GSD-12, Nod-P-1, Nod-A-1) and anthropogenic samples, measured by MC-ICP-MS. Geostand. Geoanal. Res. 29 (1), 95–106.
Cloquet, C., Carignan, J., Libourel, G., Sterckeman, T., Perdrix, E., 2006. Tracing source pollution in soils using cadmium and lead isotopes. Environ. Sci. Technol. 40, 2525–2530.
Cook, N.J., Ciobanu, C.L., Pring, A., Skinner, W., Shimizu, M., Danyushevsky, L., Saini-Eidukat, B., Melcher, F., 2009. Trace and minor elements in sphalerite: a LA-ICPMS study. Geochim. Cosmochim. Acta 73, 4761–4791.
Das, P., Samantaray, S., Rout, G.R., 1997. Studies on cadmium toxicity in plants: a review. Environ. Pollut. 98 (1), 29–36.
Duce, R.A., Liss, P.S., Merrill, J.T., Atlas, E.L., Buat-Menard, P., Hicks, B.B., Miller, J.M., Prospero, J.M., Arimoto, R., Church, T.M., Ellis, W., Galloway, J.N., Hansen, L., Jickells, T.D., Knap, A.H., Reinhardt, K.H., Schneider, B., Soudine, A., Tokos, J.J., Tsunogai, S., Wollast, R., Zhou, M., 1991. The atmospheric input of trace species to the world ocean. Glob. Biogeochem. Cycles 5 (3), 193–259.
Ettler, V., Legendre, O., Bodénan, F., Touray, J.C., 2001. Primary phases and natural weathering of old lead–zinc pyrometallurgical slag from Příbram, Czech Republic. Can. Mineral. 39 (3), 873–888.
Frost, R.L., Martens, W.N., Wain, D.L., Hales, M.C., 2008. Infrared and infrared emission spectroscopy of the zinc carbonate mineral smithsonite. Spectrochim. Acta A Mol. Biomol. Spectrosc. 70 (5), 1120–1126.
Fuge, R., Pearce, F.M., Pearce, N.J., Perkins, W.T., 1993. Geochemistry of Cd in the secondary environment near abandoned metalliferous mines, Wales. Appl. Geochem. 8, 29–35.
Gerringa, L.J.A., De Baar, H.J.W., Nolting, R.F., Paucot, H., 2001. The influence of salinity on the solubility of Zn and Cd sulphides in the Scheldt estuary. J. Sea Res. 46 (3), 201–211.
Godt, J., Scheidig, F., Grosse-Siestrup, C., Esche, V., Brandenburg, P., Reich, A., Groneberg, D.A., 2006. The toxicity of cadmium and resulting hazards for human health. J. Occup. Med. Toxicol. 1 (1), 22.
Heidel, C., Tichomirowa, M., Breitkopf, C., 2011. Sphalerite oxidation pathways detected by oxygen and sulfur isotope studies. Appl. Geochem. 26 (12), 2247–2259.
Heidel, C., Tichomirowa, M., Junghans, M., 2013. Oxygen and sulfur isotope investigations of the oxidation of sulfide mixtures containing pyrite, galena, and sphalerite. Chem. Geol. 342, 29–43.
Horner, T.J., Rickaby, R.E.M., Henderson, G.M., 2011. Isotopic fractionation of cadmium into calcite. Earth Planet. Sci. Lett. 312, 243–253.
Lacan, F., Francois, R., Ji, Y., Sherrell, R.M., 2006. Cadmium isotopic composition in the ocean. Geochim. Cosmochim. Acta 70 (20), 5104–5118.
Lambelet, M., Rehkämper, M., van de Flierdt, T., Xue, Z.C., Kreissig, K., Coles, B., Porcelli, D., Andersson, P., 2013. Isotopic analysis of Cd in the mixing zone of Siberian rivers with the Arctic Ocean—new constraints on marine Cd cycling and the isotope composition of riverine Cd. Earth Planet. Sci. Lett. 361, 64–73.
Lattanzi, P., Maurizio, C., Meneghini, C., de Giudici, G., Podda, F., 2010. Uptake of Cd in hydrozincite, $Zn_5(CO_3)_2(OH)_6$: evidence from X-ray absorption spectroscopy and anomalous X-ray diffraction. Eur. J. Mineral. 22 (4), 557–564.
Liu, J., Qu, W., Kadiiska, M.B., 2009. Role of oxidative stress in cadmium toxicity and carcinogenesis. Toxicol. Appl. Pharmacol. 238 (3), 209–214.
Martinková, E., Chrastný, V., Francová, M., Šípková, A., Čuřík, J., Myška, O., Mižič, L., 2016. Cadmium isotope fractionation of materials derived from various industrial processes. J. Hazard. Mater. 302, 114–119.
McKenna, I.M., Chaney, R.L., Williams, F.M., 1993. The effects of cadmium and zinc interactions on the accumulation and tissue distribution of zinc and cadmium in lettuce and spinach. Environ. Pollut. 79 (2), 113–120.
Nordberg, G.F., Goyer, R., Nordberg, M., 1975. Comparative toxicity of cadmium-metallothionein and cadmium chloride on mouse kidney. Arch. Pathol. 99 (4), 192–197.
Podda, F., Zuddas, P., Minacci, A., Pepi, M., Baldi, F., 2000. Heavy metal coprecipitation with hydrozincite [$Zn_5(CO_3)_2(OH)_6$] from mine waters caused by photosynthetic microorganisms. Appl. Environ. Microbiol. 66 (11), 5092–5098.

Ripperger, S., Rehkämper, M., Porcelli, D., Halliday, A.N., 2007. Cadmium isotope fractionation in seawater—a signature of biological activity. Earth Planet. Sci. Lett. 261 (3), 670–684.
Satarug, S., Baker, J.R., Urbenjapol, S., Haswell-Elkins, M., Reilly, P.E., Williams, D.J., Moore, M.R., 2003. A global perspective on cadmium pollution and toxicity in non-occupationally exposed population. Toxicol. Lett. 137 (1), 65–83.
Schmitt, A.D., Galer, S.J., Abouchami, W., 2009a. High-precision cadmium stable isotope measurements by double spike thermal ionisation mass spectrometry. J. Anal. At. Spectrom. 24 (8), 1079–1088.
Schmitt, A.D., Galer, S.J., Abouchami, W., 2009b. Mass-dependent cadmium isotopic variations in nature with emphasis on the marine environment. Earth Planet. Sci. Lett. 277 (1), 262–272.
Schwartz, M.O., 2000. Cadmium in zinc deposits: economic geology of a polluting element. Int. Geol. Rev. 42, 445–469.
Shiel, A.E., Weis, D., Orians, K.J., 2010. Evaluation of zinc, cadmium and lead isotope fractionation during smelting and refining. Sci. Total Environ. 408 (11), 2357–2368.
Shiel, A.E., Weis, D., Orians, K.J., 2012. Tracing cadmium, zinc and lead sources in bivalves from the coasts of western Canada and the USA using isotopes. Geochim. Cosmochim. Acta 76, 175–190.
Silva, G.D., Lastra, M.R., Budden, J.R., 2003. Electrochemical passivation of sphalerite during bacterial oxidation in the presence of galena. Miner. Eng. 16 (3), 199–203.
Souissi, R., Souissi, F., Chakroun, H.K., Bouchardon, J.L., 2013. Mineralogical and geochemical characterization of mine tailings and Pb, Zn, and Cd mobility in a carbonate setting (Northern Tunisia). Mine Water Environ. 32 (1), 16–27.
Street, J.J., Lindsay, W.L., Sabey, B.R., 1977. Solubility and plant uptake of cadmium in soils amended with cadmium and sewage sludge. J. Environ. Qual. 6 (1), 72–77.
Takahashi, T., 1960. Supergene alteration of zinc and lead deposits in limestone. Econ. Geol. 55 (6), 1083–1115 (1960).
Tu, G.C., Gao, Z.M., Hu, R.Z., Zhang, Q., Li, C.Y., Zhao, Z.H., Zhang, B.G., 2004. The Geochemistry and Deposit-forming Mechanism of Disperse Elements. Geological Publishing House, Beijing, pp. 69–115 (in Chinese).
Udovic, M., Lestan, D., 2009. Pb, Zn and Cd mobility, availability and fractionation in aged soil remediated by EDTA leaching. Chemosphere 74 (10), 1367–1373.
Urbano, G., Meléndez, A.M., Reyes, V.E., Veloz, M.A., González, I., 2007. Galvanic interactions between galena–sphalerite and their reactivity. Int. J. Miner. Process. 82 (3), 148–155.
Wasylenki, L.E., Swihart, J.W., Romaniello, S.J., 2014. Cadmium isotope fractionation during adsorption to Mn oxyhydroxide at low and high ionic strength. Geochim. Cosmochim. Acta 140, 212–226.
Wei, R.F., Guo, Q.J., Wen, H.J., Liu, C.Q., Yang, J.X., Peters, M., Hu, J., Zhu, G.X., Zhang, H.Z., Tian, L.Y., Han, X.K., Ma, J., Zhu, C.W., Wan, Y.X., 2016. Fractionation of stable cadmium isotopes in the cadmium tolerant *Ricinus communis* and hyperaccumulator *Solanum nigrum*. Sci Rep 6, 1–9.
Wen, H.J., Zhang, Y.X., Cloquet, C., Zhu, C.W., Fan, H.F., Luo, C.G., 2015. Tracing sources of pollution in soils from the Jinding Pb–Zn mining district in China using cadmium and lead isotopes. Appl. Geochem. 52, 147–154.
Wen, H.J., Zhu, C.W., Zhang, Y.X., Cloquet, C., Fan, H.F., Fu, S.H., 2016. Zn/Cd ratios and cadmium isotope evidence for the classification of lead-zinc deposits. Sci Rep 6. https://doi.org/10.1038/srep25273.
Wiggenhauser, M., Bigalke, M., Imseng, M., Müller, M., Keller, A., Murphy, K., Kreissig, K., Rehk ämper, M., Wilcke, W., Frossard, E., 2016. Cadmium isotope fractionation in soil–wheat systems. Environ. Sci. Technol. 50 (17), 9223–9231.
Wombacher, F., Rehkämper, M., Mezger, K., Münker, C., 2003. Stable isotope compositions of cadmium in geological materials and meteorites determined by multiple-collector ICP-MS. Geochim. Cosmochim. Acta 23, 4639–4654.
Wombacher, F., Rehkämper, M., Mezger, K., 2004. Determination of the mass-dependence of cadmium isotope fractionation during evaporation. Geochim. Cosmochim. Acta 68 (10), 2349–2357.
Yang, J.L., Li, Y.B., Liu, S.Q., Tian, H.Q., Chen, C.Y., Liu, J.M., Shi, Y.L., 2014. Theoretical calculations of Cd isotope fractionation in hydrothermal fluids. Chem. Geol. 391, 74–82.
Ye, L., Cook, N.J., Ciobanu, C.L., Liu, Y.P., Zhang, Q., Liu, T.G., Gao, W., Yang, Y.L., Danyushevskiy, L., 2011. Trace and minor elements in sphalerite from base metal deposits in South China: a LA-ICPMS study. Ore Geol. Rev. 39, 188–217.
Zhang, Y.X., Wen, H.J., Zhu, C.W., Fan, H.F., Luo, C.G., Liu, J., Cloquet, C., 2016. Cd isotope fractionation during simulated and natural weathering. Environ. Pollut. 216, 9–17.
Zhu, C.W., Wen, H.J., Zhang, Y.X., Liu, Y.Z., Wei, R.F., 2015. Isotopic geochemistry of cadmium: a review. Acta Geol. Sin. 89, 2048–2057 (English Edition).
Zhu, C.W., Wen, H.J., Zhang, Y.X., Fu, S.H., Fan, H.F., Cloquet, C., 2017. Cadmium isotope fractionation in the Fule Mississippi Valley-type deposit, Southwest China. Mineral. Deposita 52 (5), 675–686.